First Reported Detection of a Winter Continental Gamma-Ray Glow in Europe

Jakub Šlegl[1,2], Zbyněk Sokol[3], Petr Pešice[3], Ronald Langer[4], Igor Strhárský[4], Jana Popová[3], Martin Kákona[1,4], Iva Ambrožová[1], and Ondřej Ploc[1]

[1]Nuclear Physics Institute of CAS, Husinec - Řež 130, 250 68 Řež, Czech Republic
[2]Faculty of Nuclear Physics and Physical Engineering of the Czech Technical University in Prague, Břehová 7, 115 19 Prague, Czech Republic
[3]Institute of Atmospheric Physics of CAS, Boční II 1401/1a, 141 00, Prague, Czech Republic
[4]Institute of Experimental Physics of SAV, Watsonova 1935/47, 040 01 Košice, Slovakia

Correspondence: Ondřej Ploc (ploc@ujf.cas.cz)

Abstract. This study presents the first-ever ~~detection of a~~ published detection of two parallel winter continental gamma-ray ~~glow~~ glows in Central Europe, observed during a rare winter thunderstorm on Milešovka hill, Czechia. ~~Unlike typical gamma-ray glow events, which are usually linked to significant electric field increases, this unique observation reveals that no substantial electric field change was recorded during the glow, challenging existing models of thunderstorm-related radiation.~~ The combination of the hill's altitude of 837 m a.s.l. and the low altitude of the winter thunderstorm cloud resulted in an observation very near the acceleration region inside the thundercloud. The event was captured using a combination of advanced instruments, including a Ka-band cloud profiler~~and a high-energy gamma-ray spectrometer~~, which enabled detailed analysis of the storm's microphysics, SEVAN large area scintillation detector for monitoring ionizing radiation, and a manned professional meteorological observatory. The radar data indicated the alignment of ice crystals within the cloud, strongly suggesting the presence of a substantial electric field~~, despite its weak measurement on the surface. This unexpected decoupling of electric field strength and gamma-ray glow generation opens new avenues for understanding the processes driving high-energy phenomena in thunderstorms.~~. The findings offer valuable insights into winter thunderstorm dynamics in continental climates, with broader implications for ~~the study of~~ studying high-energy atmospheric physics.

1 Introduction

~~Since the first observations~~ Observations of radiation coming from thunderclouds were made onboard airplanes and balloons (McCarthy and Parks, 1985; Kelley et al., 2015; Kochkin et al., 2017) ~~, many other observations were also reported~~ as well as on the ground at locations such as Lomnický štít, ~~Musala, Aragats, Florida, Tibet, and Japan (Kudela et al., 2017; Chum et al., 2020; Šlegl et al~~ Slovakia (Kudela et al., 2017; Chum et al., 2020; Šlegl et al., 2022; Chilingarian et al., 2021c), Musala, Bulgaria (Chilingarian et al., 2021c , Aragats, Armenia (Chilingarian et al., 2021c, b, 2016; Chilingarian and Mkrtchyan, 2012; Chilingarian et al., 2010; Williams et al., 2022 , Yangbajing, Tibet, China (Tsuchiya et al., 2012), and Japan (Tsuchiya et al., 2007, 2009, 2011; Torii et al., 2009, 2011; Wada et al., 2021b .

Gamma-ray glows, also called long bursts (Tsuchiya et al., 2009; Torii et al., 2011) or thunderstorm ground enhancements (Chilingarian et al., 2011), are minute-scale long enhancements in the ionizing radiation environment with passing thunderclouds. The mechanisms of their origin are attributed to the process called relativistic runaway electron avalanche (RREA) (Gurevich et al., 1992) and to the modification of the energy spectra (MOS) (Chilingarian and Mkrtchyan, 2012) created between regions of opposite charge strong enough, with at least one situated in the cloud.

This region of strong electric field (charged region) moves with the cloud and creates typical bell-shaped enhancements in the count rates observed by ground detectors (Wada et al., 2021b). The peak of count rates is detected at the moment of the shortest distance between the detector and the center of the active (charged) region.

In some cases, such as the presented event, the gamma-ray glow is terminated by discharge. This discharge reduces at least one of the charged regions and makes the RREA or MOS process stop. Many such cases have been reported (Tsuchiya et al., 2013; Chilingarian et al., 2015, 2017), with discharges sometimes starting far from the detected gamma-ray glow where the intra-cloud (IC) leader passed by (Wada et al., 2018, 2019).

Winter thunderstorms are much rarer, especially in continental Europe. During 4 years of continuous measurements on top of the Milešovka hill, only a few summer season gamma-ray glows were observed (Kolmašová et al., 2022), and none during winter until the event observed on February 4, 2022, which is presented here. This is probably caused by several reasons: winter continental thunderstorms are rare (there are known occurring winter thunderstorms near the coast of Japan, near the Great Lakes and in the Mediterranean, all connected to water), they are of low intensity (low flash rate), and their cloud base is higher than in Japan, so that the photons from bremsstrahlung is attenuated bellow detectable level. Other reason is that the measurements of ambient ionizing radiation were not suitable for such observations with too long acquisition intervals (10 minutes for Czech radiation monitoring system - (**?**)).

For the study of thunderstorms, the observatory on the Milešovka hill (837 m a.s.l.) was equipped with a unique set of measuring instruments for the detection of ionizing radiation, meteorological and climatological observations, including the cloud profiler (Ka-band).

2 Detectors and Data

Milešovka station (50.55° N, 13.93° E), Czech Republic, is a professional meteorological station with a 24/7 service located at the top of the Milešovka hill at an altitude of 836 m a.s.l. It exceeds the surrounding area by about 300 meters.

Apart from standard meteorological and climatological measuring instruments (thermometer, barometer, rain gauges, hygrometer, wind speed and direction meters), the station is also equipped with a ceilometer, disdrometer, Ka-band cloud profiler, and radiation ~~detectors SEVANwith a gamma-ray spectrometer Georadis RT-56~~detector SEVAN.

The ~~Georadis **RT-56** spectrometer includes a 3" × 3" cylinder BGO crystal coupled with a photomultiplier tube (PMT) and electronics for data acquisition. The primary spectrum starts at 0 and spans up to 4.5 MeV with 1500 channels separated by 3 keV. The calibration is regular and automatic, based on naturally abundant isotopes.~~

~~The cosmic mode of the spectrometer stores information on deposited energies higher than the primary spectrum, while the measuring mode is the Time-over-Threshold mode, with a threshold of 4.05 MeV calibrated by peak shape fits. The RT-56 spectrometer also calculates the number of pileups per second and contains a GPS module. The spectrometer is able to provide a timestamp of up to 4000 particles every second in a selected energy interval. In the case of the winter thunderstorm on February 4, 2022, studied in this paper, it was set up to 4.5 MeV.~~

~~Another important feature of the detector are its internal batteries which ensure uninterrupted measurements during thunderstorms when blackouts are common, especially in mountainous areas. The batteries of the detector at the Milešovka station can maintain the full detector operation for up to one day.~~

~~The second ionizing radiation detector used in this study is the~~ **SEVAN** detector system (Chilingarian et al., 2009) ~~, which~~ consists of three plastic scintillator detectors, each coupled with one PMT. The upper one as well as the bottom one are set up from four plastic scintillator slabs (with thickness of 5 cm) creating a square with one-meter long sides. The middle one, separated from the top one and the bottom one by a 5 cm thick lead, consists of five stacked slabs (with thickness of 5 cm each). The energy threshold of the upper channel of SEVAN is expected to be approximately 7 MeV.

This set-up allows, together with fast electronics, to estimate particle types as well as their intensity. For example, coincidence 100 (response in the upper channel while no response in the bottom and middle channels in a narrow time interval) shows interactions of most probably photon or electron. Coincidences 101 and 111 show most probably muons as they pass through both lead layers.

~~**Electric field mill Boltek EFM-100C** manufactured by the Boltec company measures the electrostatic field in a vertical direction. It is oriented downwards (inverted position) to minimize the precipitation noise. Its negative values mean that the electric field's direction is upwards and electrons are accelerated downwards. The sampling frequency is 20 Hz~~The SEVAN detector provides only count rates per second.

Cloud profiler MIRA 35c at the Milešovka station is a vertically oriented Doppler polarimetric radar manufactured by the METEK GmbH company. It operates within Ka-band with a center frequency of ~~35.12 ± 0.1~~ 35.12 ± 0.1 GHz and a peak power of 2.5 kW. The temporal resolution is 2 s and vertical resolution includes 509 gates separated by 28.8 m. More technical details are given in Sokol et al. (2020) and Kolmašová et al. (2022). Data provided by the cloud profiler~~are ~~, which are used in this study, are radar reflectivity (Ze), Doppler vertical velocity (V), its spectrum width (W), ~~spectrum width, ~~Linear Depolarization Ratio (LDR), and co-polar correlation coefficient (RHO).

Cloud radars differ from conventional operational radars in that they use significantly higher frequencies than operational weather radars (usually working in C-, S- or X-band). This is reflected in the measurement characteristics. Contrary to operational weather radars which record and recognize bigger (precipitation) particles, cloud radars can measure fine particles, such as cloud droplets or ice crystals thereby enabling individual hydrometeor distinction. Further, cloud radars generally have much higher spatial resolution as compared to operational weather radars. In contrast, the measurements of cloud radars are more affected by attenuation by heavy rain and the radar beam reflections follow Mie scattering rather than Rayleigh scattering, which influences the processing of e.g., Ze. The Ka-band cloud radar at the Milešovka station emits energy in the horizontally polarized plane but receives reflections in both the horizontal (Zh; co-channel) and vertical (Zv; cross-channel) planes. The

LDR, which is the ratio of Zv to Zh, allows determining the symmetry of the measured object (its shape), which contributes significantly to distinguish the type of a hydrometeor present in a cloud.

V determines the velocity of the object in the radial direction and W characterizes the variability of the velocity of moving hydrometeors. Since the measurements are made in the vertical direction and individual hydrometeors have different terminal velocities, high values of W indicate the existence of different hydrometeors in the scan volume. The value of RHO depends on the symmetry/shape of the hydrometeors and high RHO values correspond to symmetric objects.

Postprocessing of the data was carried out ~~with~~ following the methods described in Sokol et al. (2018)~~which also calculates~~. It consists of calculating vertical air velocity (Va)~~and provides hydrometeor classification~~, which is then used in the classification of hydrometeors developed and described in the paper.

Disdrometer Thies Laser Precipitation Monitor with an infrared laser beam is capable of distinguishing the type of hydrometeors by their size and fall speed.

Lightning data recorded by the **EUCLID** (European Cooperation for Lightning Detection, https://www.euclid.org/) network by BLIDS (Blitz Informationsdienst von Siemens), used in this paper, contain records of the time (with the accuracy of ms), position, type (Cloud-to-Cloud, CC; or Cloud-to-Ground, CG), estimated peak current (in kA including its polarity), and quality of detection (good/bad) of registered discharges. It should be mentioned that all lightning data for the studied winter storm were of good quality.

Blitzortung, a lightning detection network for localization of atmospheric discharges with very low-frequency receivers (3 to 30 kHz), uses the Time of Arrival and Time of Group Arrival techniques to register lightning discharges (Wanke, 2010). As the Milešovka hill is in the area of a dense coverage of antenna stations, ~~we believe that~~ the accuracy of this network is within 1 km in the area, as the Blitzortung project claims.

3 Results

3.1 ~~Meteorological Situation~~Gamma-Ray Glows

~~Winter thunderstorms in the Czech Republic, a landlocked country, are rare. Munzar and Franc (2003) mentioned a rise in the number of winter thunderstorms over the whole Czech Republic but not more than a couple per year. Unlike summer storms, the winter thunderstorms cause less economic damage but are more unpredictable compared to summer thunderstorms.~~

~~Munzar and Franc (2003) also related the occurrence of winter thunderstorms over the Czech Republic with cold fronts. This was also the case on February 4, 2022 (see Figure 7), when~~ During the passing thunderstorm, two different gamma-ray ~~glow was measured by two detectors. The cold front with temperatures below zero passes the Milešovka hill with a cloud base below the station at the moment of the~~ glows were detected. A very obvious one, with a shorter duration and higher intensity, ended by a discharge - we will call it a strong gamma-ray ~~glow event.~~ glow. A longer duration, with less intensity and not ended by a discharge - we will call it a weak gamma-ray glow. This naming only refers to the detected count rates as we are unaware of the true gamma-ray glow intensity at its maximum outside the station. Temporal positions of those gamma-ray glows are indicated

on Figure **??** by different levels of gray: strong gamma-ray glow is indicated by darker grey, whereas weak gamma-ray glow by lighter gray.

As the function $F(t)$ to fit temporal evolution of count rate a Gaussian curve was selected as in Wada et al. (2021b):

$$F(t) = \sum_{i=1}^{2} a_i \exp\left(\frac{-(t-\mu_i)^2}{2\sigma_i^2}\right) + c, \quad (1)$$

where t is time, a is the peak count rate, μ is the peak time, σ is the standard deviation, and c is the background count rate. Gaussian function was selected only because the time series of count rates roughly follow this line. However, here is no physical explanation. This function has a benefit of easy calculation of Full duration in half maximum ($FDHM \approx 2.355\sigma$).

3.1.1 Strong Gamma-Ray Glow

The rise in the upper SEVAN channel lasted for 30 seconds and reached a maximum of 835 counts per second (i.e., 375% of the background level). The peak occurred 8 seconds before the end with the discharge, that happened between 23:20:08.147 and 23:20:08.187, according to the Blitzortung network. Throughout the paper, we will use time in UTC, local time (CET) is UTC+01.

~~According to the Blitzortung network data,~~ As visible in Figure 1, the count rates follow the Gaussian curve up to the maximum of the strong gamma-ray glow, being still at the beginning of the Gaussian curve. However, our fitting is relevant because the fitted curve is similar to those previously observed in e.g., Šlegl et al. (2022); Wada et al. (2019). If the strong gamma-ray glow had not been interrupted by the discharge and had continued following the Gaussian curve, the ~~thunderstorm lightning activity started in Germany, near Dortmund, around 17:~~duration of the peak would have been roughly 2.5 minutes, which aligns with the previous observations as the wind speed of 10 m/s does not deviate from regular wind speed during thunderstorms (with higher speed the acceleration region moves faster and thus creates a narrower peak). Also, the peak count rate of 5552 counts/s for SEVAN top channel with subtracted background is reasonable as the cloud base height was less than 30 ~~UTC. It crossed Germany and reached the German-Czech borders and the Ore Mountains at 22:50 UTC, then crossed the Milešovka station and eventually dissipated after the last discharge east of the Milešovka hill at 23:23 UTC (see Figure 2).~~ meters (the lower the accelerating region the lower the attenuation of the radiation). There were even higher detected count rates of SEVAN top channel on Lomnický štít, Slovakia (Chum et al., 2020).

~~Discharges detected by Blitzortung (black-bordered circles) and EUCLID (yellow-bordered circles) at the time of the end of the gamma-ray glow (23:20:08.147-187, blue scale) and 3 minutes later (23:23:03.300-450, reddish scale). Color scales show time in milliseconds from the first discharge. Both networks indicate the beginning of the gamma-ray ending discharge very near to the Milešovka station depicted by a red-bordered circle.~~

4 ~~Results~~

3.1 ~~Discharge Ending Gamma-Ray Glow~~

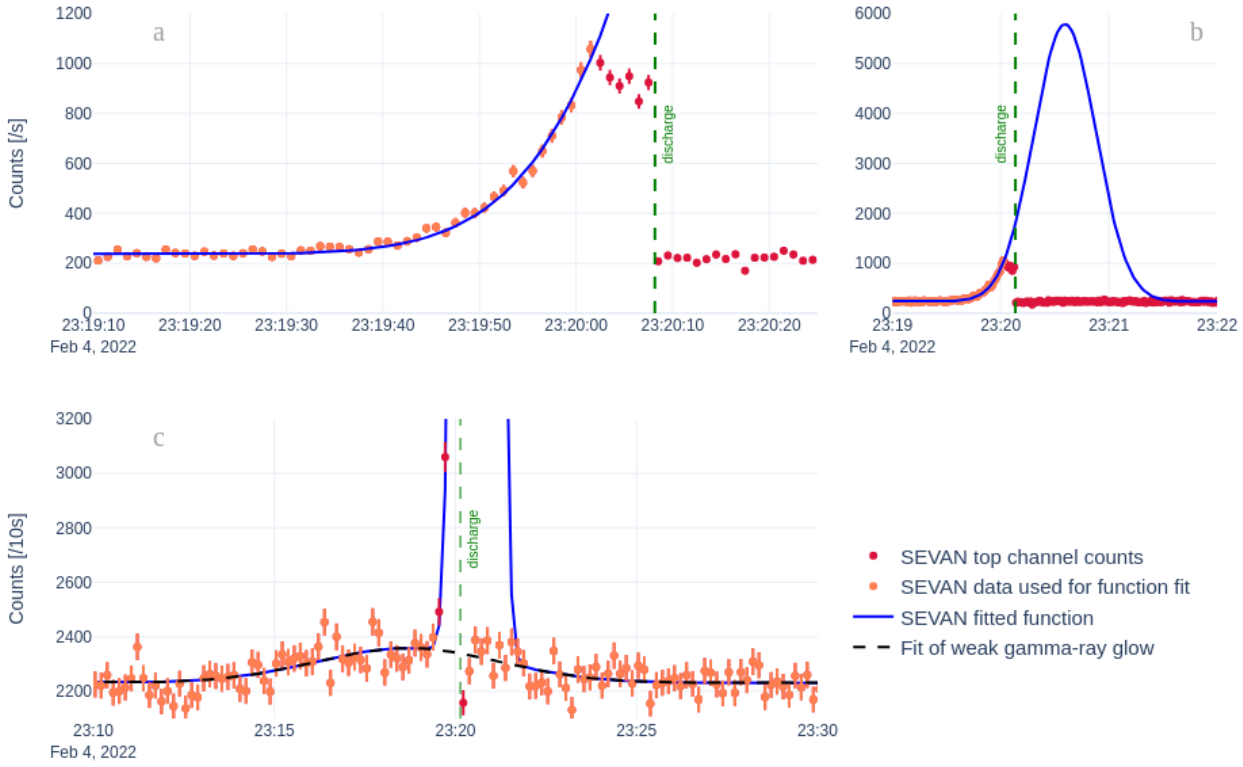

Figure 1. ~~Change in 2 m temperature~~ Counts measured by the upper channel of SEVAN (~~top left~~red) ~~, dew point at 2 m~~ without considering coincidences. Panel (~~top right~~a) ~~, pressure~~ shows the strong gamma-ray glow fitted with the best fit function (~~bottom left~~light markers depict data used for the function fitting, while dark markers represent data not used for the fitting). Two Gaussian functions were combined, one for weak gamma-ray glow and ~~cloud base height~~ one for strong, 1. Panel (~~bottom right~~b) ~~during~~ represents the ~~thunderstorm on February 4~~expected peak had there not been any discharge resulting from the best fit functions. Panel (c) shows SEVAN data for the weak gamma-ray glow and its best fit function in 10 s summed bins (light markers represent data used for the function fitting, ~~2022.~~ while dark markers display data not used for the dashed function fitting). Note that two markers of the ~~cloud base height is at~~ strong gamma-ray glow are out of the ~~lowest measurable value at 23:20 UTC. The actual cloud base was below~~ y-axis range of the ~~observation site~~graph.~~Solid lines only connect points of measurements for better readability. Gamma-ray glows are represented by gray areas.~~

~~Gamma-ray glow observed by both SEVAN and RT-56 spectrometer. SEVAN top channel (red), RT-56 all counts/s (blue), RT-56 counts/s of photons with energy above 3 MeV (yellow), RT-56 detected pile-ups (green), near surface electric field measured by Boltek EFM-100c (cyan). Note that the gaps in data of RT-56 were caused by a software error in timing from GPS.~~

~~During~ The continuation of the gamma-ray glow, ~~there was only a weak electric field measured by the electric field mill. The electric field data also surprisingly show that there is no sudden detected change of electric field with the discharge. Usually during the discharge, the data from electric field mills show a sudden change~ if not terminated by the discharge, would correlate to the echo of aligned ice crystals by the electric field, as shown by the data from the Cloud profiler (Figure 8 - RHO). The continuation of such alignment of ice crystals in the upper part of the cloud can be explained by residually charged areas in the upper part of the cloud, above which the ice crystals were still caught in the electric field~~towards the opposite polarity with rapid exponential restitution, but that was not the case during the winter thunderstorm on February 4, 2022. This could be due to some frost on the electric field mill and its location close to vegetation (trees are in close vicinity of the electric field mill).~~ Either the stroke did not discharge the upper charged region totally or not at all. This suggests the possibility of a horizontal discharge that left the upper charged region intact.

A question arises about the last 7 seconds (23:20:01.0-23:20:08.0) that preceded the discharge. As it does not follow the Gaussian curve, some mechanism must have prevented the gamma-ray glow from its full development. Such a sharp peak with a decrease before the end of the discharge was also observed by Wada et al. (2019).

3.0.1 Discharge Ending the Strong Gamma-Ray Glow

The discharge was accompanied by strong light and sound emissions. The observer on duty at the Milešovka station reported no observable time difference between the lightning and the thunder. This shows the extreme proximity of the ~~discharge~ flash to the station, as supported by Blitzortung and EUCLID data. Shortly after the ~~discharge~~flash, the power generator automatically started, suggesting a direct hit to the facility or a nearby strong electric impulse that caused a power outage.

The EUCLID network reported two ~~discharges~ radio-frequency pulses of the same flash (See Figure 2) very close to the station (-3.4 and -9.8 kA, both identified as CC). Blitzortung recorded multiple ~~discharges~ pulses within a radius of 11 km from the station but noted that they began near the station as well. The ~~discharge,~ lightning flash ending the gamma-ray glow ~~,~ lasted for about 40 ms (23:20:08.147-187 UTC). According to the lightning monitoring networks (both EUCLID and Blitzortung), the ~~discharge~ lightning flash occurred in very close proximity to the Milešovka station. EUCLID even showed a horizontal distance of 50 m from the station, while it was 1.1 km in the case of Blitzortung. Both networks recorded the same time of the ~~discharge~ first radio-frequency pulse and indicated the continuation of electromagnetic activity at 23:20:08.163. EUCLID showed one more ~~discharge~~pulse, very close to the Milešovka station; however, Blitzortung recorded 21 ~~discharges~ pulses in the vicinity of the station (within a 3 km distance) and two further, 15 and 18 km away from the station, respectively. The following ~~discharges~ radio-frequency pulses were observed by Blitzortung only (one at 23:20:08.182 and two at 23:20:08.187).

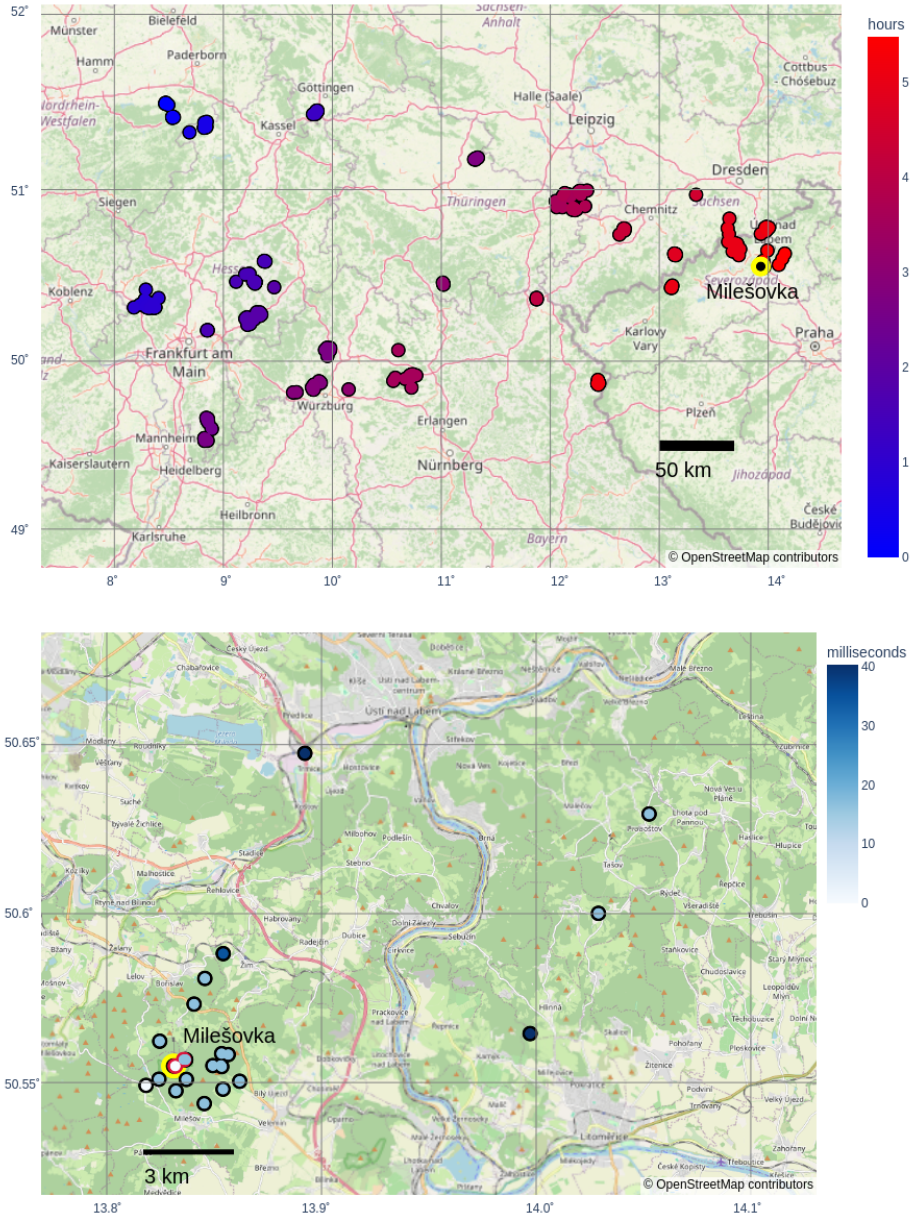

Figure 2. Top: Radio-frequency pulses detected by Blitzortung (black-bordered circles) as the thunderstorm passed Germany and entered Czechia. Color scale shows time in hours from the first flash at 17:51:01. Milešovka event happened at the final stage of the thunderstorm. Bottom: Radio-frequency pulses detected by Blitzortung (black-bordered circles) and EUCLID (red-bordered circles) at the time of the end of the strong gamma-ray glow (23:20:08.147-187). Color scale shows time in milliseconds from the first pulse of the flash. Both networks indicate the beginning of the gamma-ray ending flash (its first radio-frequency pulse) very near the Milešovka station depicted by a yellow-bordered point. © OpenStreetMap contributors 2024. Distributed under the Open Data Commons Open Database License (ODbL) v1.0.

~~For a detailed analysis of the thunderstorm on February 4, 2022, please refer to Popová et al. (2023).~~ According to the analysis of Kolmašová (2024) the gamma-ray ending discharge was probably an upward-going lightning stroke initiated at the observatory tower.

3.1 ~~Electric Field~~

~~The weak electric field measured during the~~

3.0.1 Weak Gamma-Ray Glow

Upon inspection closer through the data, a weak gamma-ray glow can be seen in the SEVAN top channel data, Figure 1c. A 10-second binning was used for better visibility. The discharge did not end this gamma-ray glow as the strong one. A Gaussian curve fits its shape, and from that it is seen that it's much broader in duration (FDHM was 6 minutes) than the strong gamma-ray glow~~(see Figure ??) can be explained in several ways. One possibility is that the charge region was partially neutralized by an opposite charge, resulting in an integrated value measured beneath the cloud that shows only low values. Such an arrangement could occur, for example, if the charge is oriented vertically rather than horizontally, as indicated by calculations in Popová et al. (2023). Alternatively, this finding could suggest a more complex charge structure, which aligns with previous studies Brothers et al. (2018). Such a complex structure may lead to ground measurements failing to capture the strong fields present in the upper cloud layers, thereby explaining the weak electric field recorded during the~~ , and its center (23:18:40) is even before the start of the strong glow. In the following figures, it is marked by a light grey color.

Different behaviors of the weak gamma-ray ~~glow.~~ glow from the strong one lead us to the suggestion that the source of the glow was different. The strong gamma-ray glow source was very near the observatory and probably above it as the flash of lightning started above the station. The weak gamma-ray glow, on the other hand, was probably way off as it was very weak in detected count rates and also was not discharged. With the presence of the strong gamma-ray glow and small height of the cloud, we believe the source of the weak gamma-ray glow was moving sideways of the observatory.

As the flash ending strong gamma-ray glow propagated in the north-east direction along the front, we can place the source of the weak gamma-ray glow in the area south of the hill. A storm center passing just south of the observatory seems to be separated by the Milešovka hill from the north/discharged one, see Figure 3. It is possible that this south center was separated enough not to get discharged.

This thunderstorm center can be also observed on the cross section 0 on the Figure 4. This area of strong reflectivity (40-45 dBZ) is reaching to the bottom of the radar vertical limit at 450 m above the ground and has a horizontal offset of 500 m from the station.

3.1 Meteorological Situation

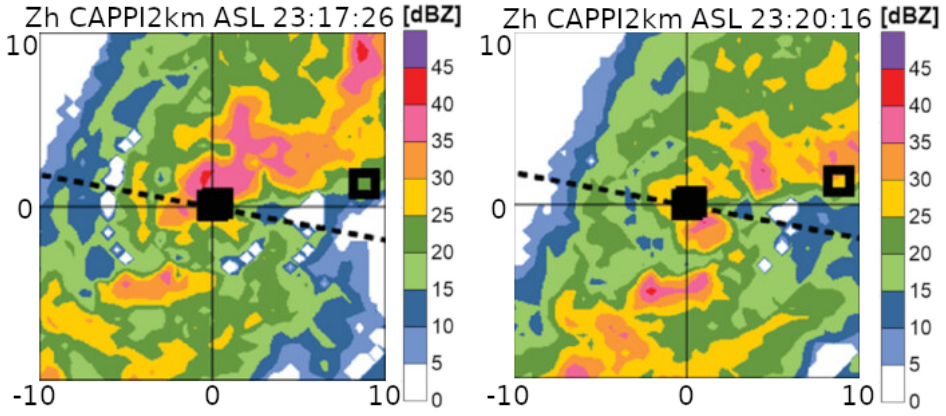

Figure 3. Radar reflectivity factor fields of horizontal polarization wave Zh at constant altitude plan position indicator (CAPPI) 2 km ASL during the winter thunderstorm adopted from Popová et al. (2023). The time of the beginning of plan position indicator (PPI) scans is shown in the title. The black square in the center of the panels indicates the position of the Milešovka observatory and the axes show the distance from the observatory in kilometers. The dashed line shows the movement of the cold front.

Winter thunderstorms in the Czech Republic, a landlocked country, are rare. Munzar and Franc (2003) mentioned a rise in the number of winter thunderstorms over the whole Czech Republic but not more than a couple per year. Unlike summer storms, the winter thunderstorms cause less economic damage but are more unpredictable compared to summer thunderstorms.

Munzar and Franc (2003) also related the occurrence of winter thunderstorms over the Czech Republic with cold fronts. This was also the case on February 4, 2022 (see Figures 7 and 5), when gamma-ray glows were measured. The cold front with temperatures below zero passes the Milešovka hill with a cloud base below the station at the moment of the gamma-ray glow event. The passage of the cold front is confirmed by the synoptic map (Fig. 5) and the radar reflectivity at the CAPPI 2km level (Fig. 6) from the operational radar of the Czech Hydrometeorological Institute. The front was moving from the northwest and the radar reflectivity (Fig. 6) shows that there were several storm centres on the front accompanied by lightning.

According to the Blitzortung network data, the thunderstorm lightning activity started in Germany, near Dortmund, around 17:30 UTC. It crossed Germany and reached the German-Czech borders and the Ore Mountains at 22:50 UTC, then crossed the Milešovka station and eventually dissipated after the last flash east of the Milešovka hill at 23:23 UTC (see Figure 2). Overall flash rate was 7.5 flashes per hour.

3.2 Cloud Profiler Data and Disdrometer

The thunderstorm passing the Milešovka station on February 4, 2022, was unique in its height. The cloud base was unusually low—at the altitude of the hilltop or even lower—and the cloud top was also low. As visible in the data from the cloud profiler (Figure 8), the height of the cloud top did not exceed 3500 m above the hilltop. The cloud top height was also estimated using ~~satellite measurements of~~ Meteosat Second Generation ~~(), not shown here~~satellite (https://www.eumetsat.int/meteosat-second-generation).

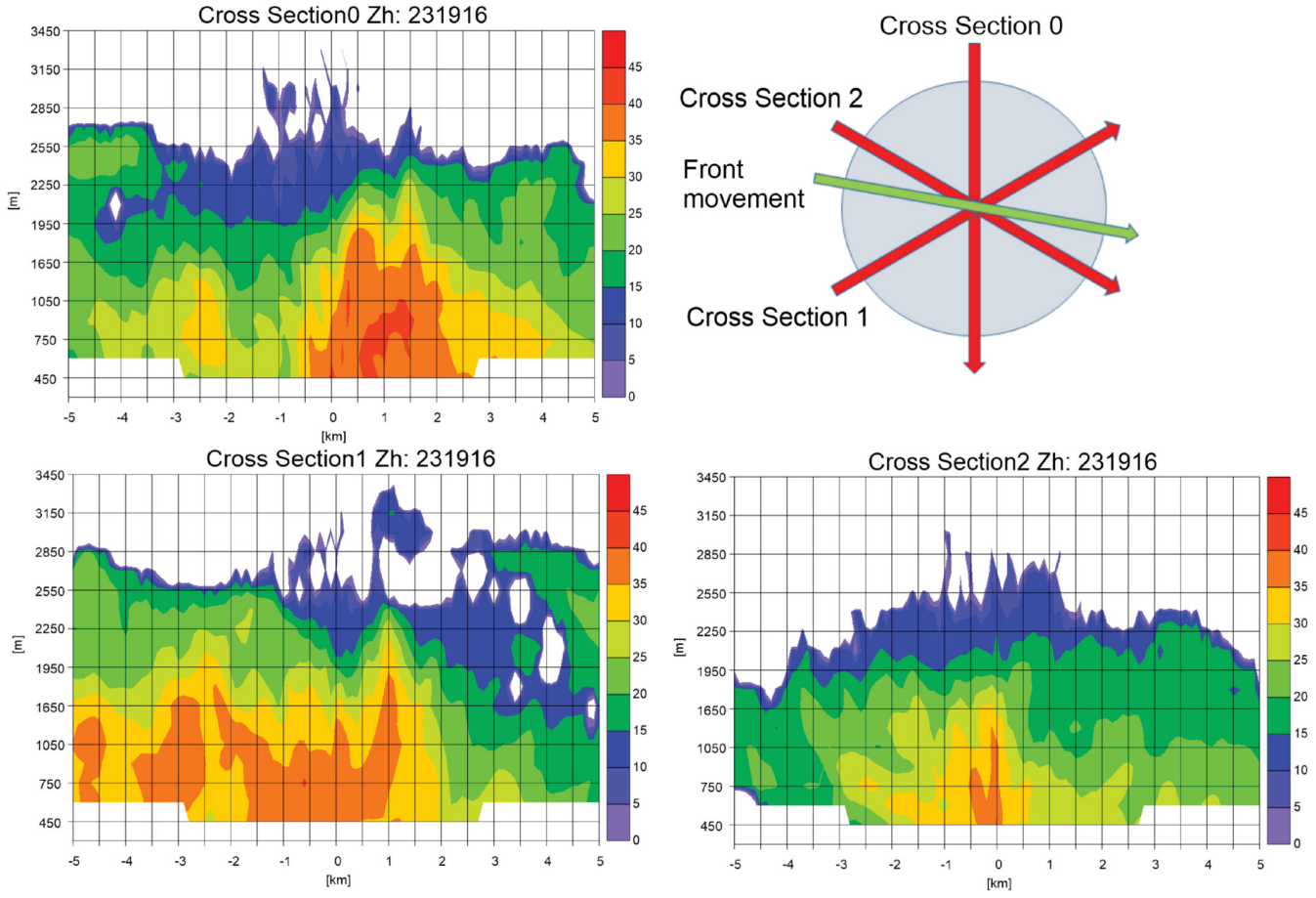

Figure 4. Vertical cross-sections of Zh at 23:19:16 UTC (RHI scans). Red arrows in the upper-right panel show the orientations of the cross-sections, while the green arrow in the upper-right panel shows the approximate movement of the cold front (i.e. cloud belt) at constant altitude plan position indicator (CAPPI) 2 km. The direction of the cold front corresponds to the wind direction measured at the surface at the time of the recorded lightning. The radar position is at (0,0). Figure is adopted from Popová et al. (2023).

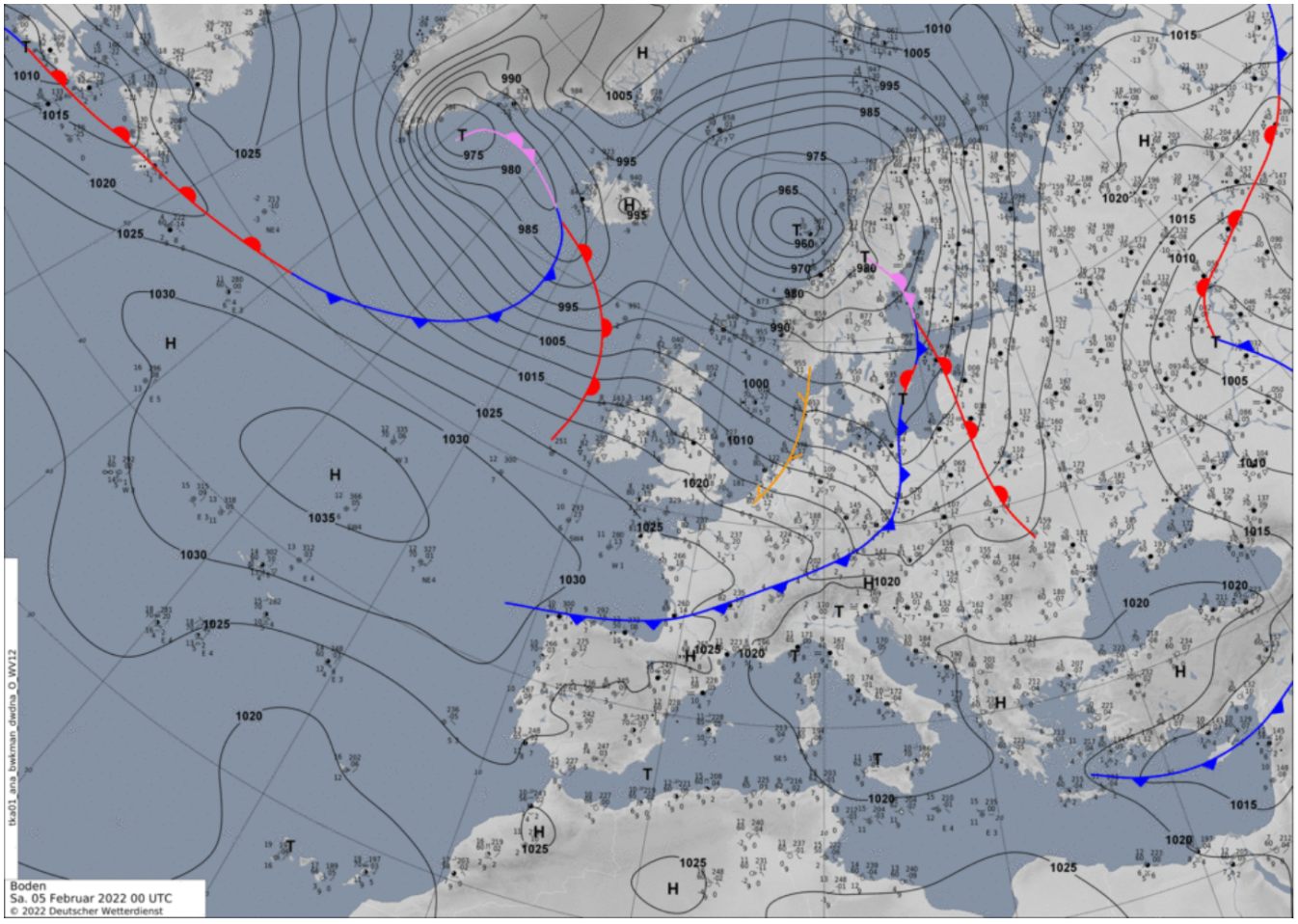

Figure 5. Synoptic map based on reanalysed data provided by German Weather Service (DWD).

Using the brightness temperature of the infrared channel 10.8 μm at 23:20 UTC and the temperature sounding measurements at the Praha-Libuš station (80 km southwards from the Milešovka observatory) at 00:00 UTC on February 5, 2022, the cloud top height was approximately 3 km above the surface (Popová et al., 2023). LDR and RHO values (Figure 8) show that the height of the thundercloud reflecting back the signal was even smaller, reaching a height of only 2500 m at the maximum and only 1500 m at the time of the discharge.

~~Throughout the storm, we observed a low-intensity~~

The weak gamma-ray glow ~~that~~ started at the moment of a higher reflectivity region with Ze above 15 dBZ started passing the hill and ended when there were very low values of Ze (lower than -15 dBZ; Figure 8 - Ze). The end of the ~~low-intensity~~ weak gamma-ray glow roughly correlates with the last pixel of graupel and hail (GH), see Figure 9, as deduced from the fitted Gaussian curve, but since the excess of the ~~low-intensity~~ weak gamma-ray glow was low above the background, its end is not very recognizable and is smeared in the fluctuation of the background. During the ~~low-intensity~~ weak gamma-ray glow, the

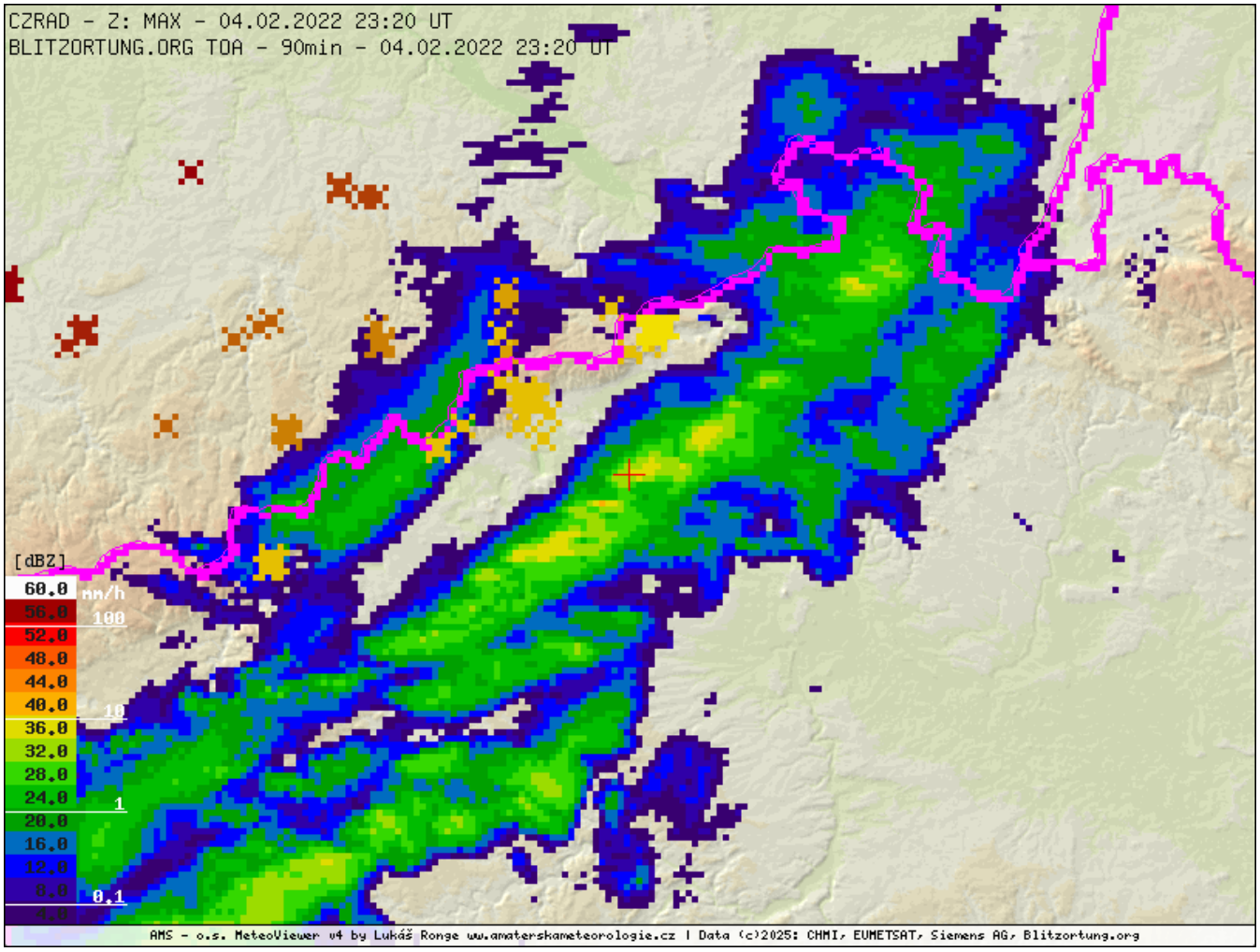

Figure 6. Radar reflectivity at constant altitude plan position indicator (CAPPI) 2km ASL in dBz measured by the radar network CZRAD operated by the Czech Hydrometeorological Institute. The red cross indicates position of Milešovka hill. The pink line displays a border of the Czech Republic, Germany and Poland.

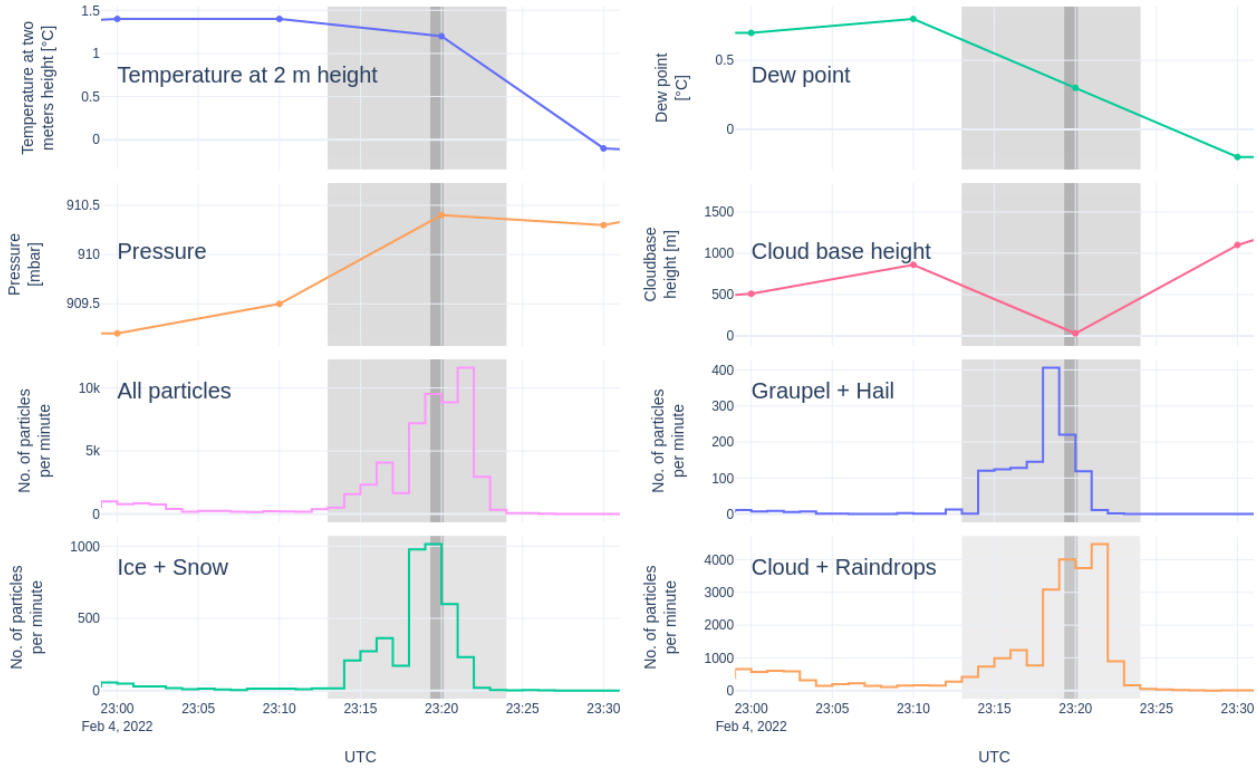

Figure 7. Change in 2 m temperature, dew point at 2 m, pressure, cloud base height, number of all particled detected by disdrometer, and three groups of hydrometeors detected by the disdrometer: graupel + hail (but there was no hail), ice and snow, and cloud and raindrops during the thunderstorm on February 4, 2022. Note that the cloud base height is at the lowest measurable value at 23:20 UTC. The actual cloud base was below the observation site. Solid lines only connect points of measurements for better readability. Gamma-ray glows are represented by gray areas.

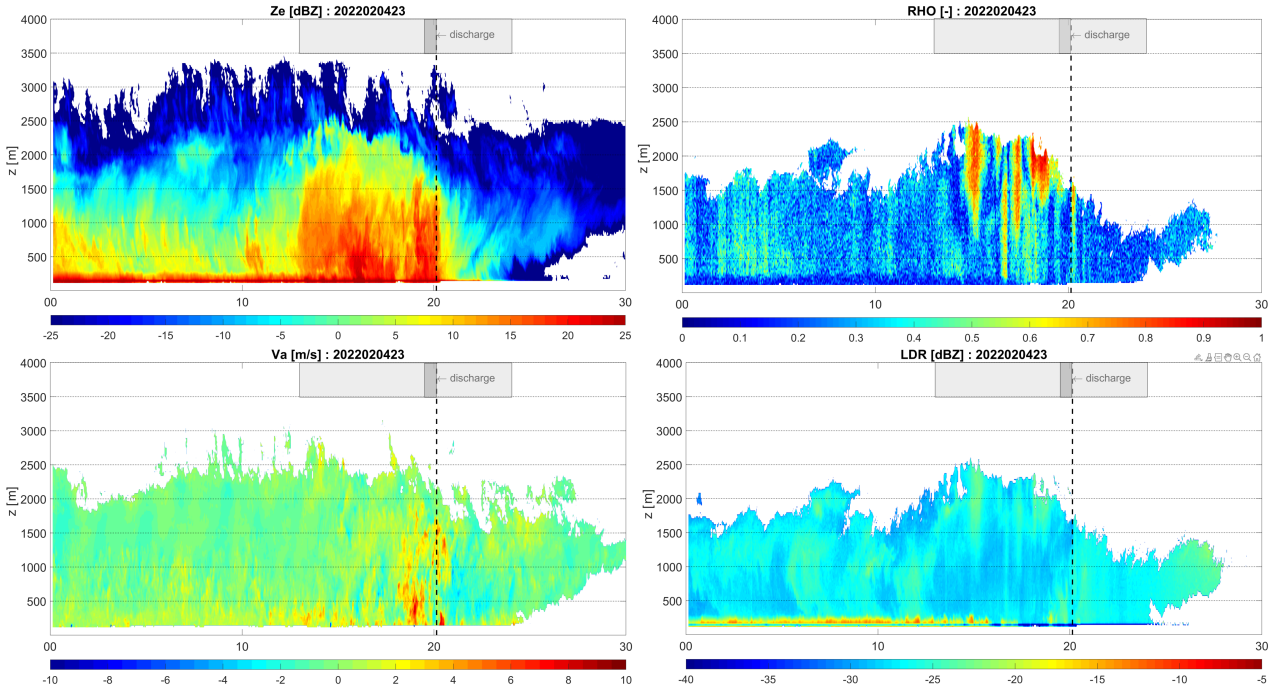

Figure 8. *Ze*, *LDR*, *Va*, and *RHO* measured by the vertical profiler MIRA 35c from 23:00 to 23:30 UTC (horizontal axis). The vertical dashed line shows the time of the recorded discharge. Gray areas show both gamma-ray glows: low-intensity gamma-ray glow (light gray), high-intensity gamma-ray glow ended by the discharge (dark gray). For more details see Popová et al. (2023).

cloud contained graupel and hail with a sparse mix of cloud water and raindrops (Figure 9). The classification algorithm has one class for both hail and graupel. Due to the lower values of the measured Ze, it can be concluded that hail probably did not occur ~~.~~ as is supported by the data from disdrometer, see Figure 7.

~~During the storm, we also observed a shorter strong gamma-ray glow, which ended by the discharge.~~ During the strong gamma-ray glow, Ze was above 20 dBZ in the lowest 1500 m of the cloud, and the cloud contained a category of hydrometeors of graupel and hail with a sparse mix of cloud water and raindrops, as in the case of the low-intensity gamma-ray glow. These findings are consistent with ranges previously calculated by Chilingarian et al. (2021b); Diniz et al. (2022).

The polarimetric feature of the cloud profiler can even reveal areas of aligned ice crystals that change the reflection of the radar signal. This alignment is probably caused by the ambient electric field, which can be used to identify strong electric fields in clouds (Melnikov et al., 2019). In the upper parts of the cloud, the ice crystals are usually columnar in shape. If these crystals are oriented horizontally along the long axis, then Zh is larger and Zv smaller than when the crystals are oriented vertically. Hence, the LDR is higher in the latter case than in the former case. Usually ice crystals are randomly oriented in the scan volume, but when these crystals are exposed to a strong electric field, they arrange along the longer axis vertically making the

LDR to increase, and since they are symmetric in the scan direction, it makes the RHOHV to increase as well. Such areas are visible in Figure 8 - LDR, where LDR values higher than -20 dBZ indicate the alignment of ice crystals in the area above the melting layer, which shows the highest LDR values at about 250 m above the radar. These areas are even more pronounced in the projection of RHO; the higher the number, the higher the specific reflectivity leading to a conclusion on intensified electric fields (Melnikov et al., 2019). The most interesting area is just after the discharge (discharge depicted by the dashed line in Figure 8). The narrow area of higher values of RHO right after the discharge spanned from the top to almost the bottom of the cloud. This could confirm the previous existence of an area of intensified electric field that aligned the ice crystals and also caused the gamma-ray glow observed on the ground.

~~Disdrometer data around gamma-ray glows (gray vertical areas - light gray for the low-intensity glow, dark gray for the strong glow) shown as number of particles per minute: Number of all particles, Particles < 0.15 m/s, Solid precipitation, Big graupel, Small graupel, Snow grains, Rain, Small rain, Drizzle, no hydrometeor. The horizontal axis is the time in UTC.~~

Around the gamma-ray ~~glow~~ glows event, the disdrometer did not detect any hail. On the other hand, graupel and snow grains were recorded right before the strong ionizing radiation enhancement, Figure 7. The existence of falling snow grains was also recorded by the observer on duty and agrees well with the observations in other studies (Chilingarian et al., 2021a; Wada et al., 2021b).

3.3 ~~Strong Gamma-Ray Glow~~

~~The strong gamma-ray glow was detected with both the SEVAN and RT-56 spectrometer. This indicates high reliability of the results, as both detectors employ different electronics. The SEVAN detector shows the rise in the upper channel only, which indicates a low presence of high-energy photons that are able to penetrate the 5 cm thick layer of lead and thus would have been visible in the two other channels (middle and bottom one).~~

~~The rise in the upper SEVAN channel lasted for 30 seconds and reached a maximum of 835 counts per second (i.e., 375% of the normal level). The peak occurred 8 seconds before the end of the discharge, and the gamma-ray glow ended due to the lightning discharge between 20:20:08.147 and 20:20:08.187, according to the Blitzortung network.~~

~~The rise on RT-56 was 346 counts per second (i.e., 83% of the normal level). The spectrometer experienced issues with time determination, but we were able to recover most of the gamma-ray glow data. The data acquisition stopped 3 seconds before the discharge, and at that time, a huge number of pileups was detected (125 compared to approximately 7 when there was no gamma-ray glow). The exact pileup peak and its time are uncertain as it might have been reached during the data acquisition gap. High numbers of pileups per second were also observed by this detector during other events when a lightning discharge was recorded in close proximity to the detector, e.g., 2022-06-24, 2023-07-29, and 2024-07-10. Never in such a high number, though. Whether the pile-up peak can be a detection of stepped leader x-ray pulses, terrestrial gamma-ray flash, or an electronic artifact remains a question.~~

~~Counts measured by RT-56 (blue) and by the upper channel of SEVAN (red). Panel (a) shows a big gamma-ray glow fitted with the best fit function (light markers depict data used for the function fitting, while dark markers represent data not used for the fitting). For RT-56, the data were fitted with a simple Gauss function, whereas for SEVAN, we combined two Gauss~~

~~*Ze*, *LDR*, *Va*, and *RHO* measured by the vertical profiler MIRA 35c from 23:00 to 23:30 UTC (horizontal axis). The vertical dashed line shows the time of the recorded discharge. Gray areas show both gamma-ray glows: low-intensity gamma-ray glow (light gray), high-intensity gamma-ray glow ended by the discharge (dark gray). For more details see Popová et al. (2023).~~

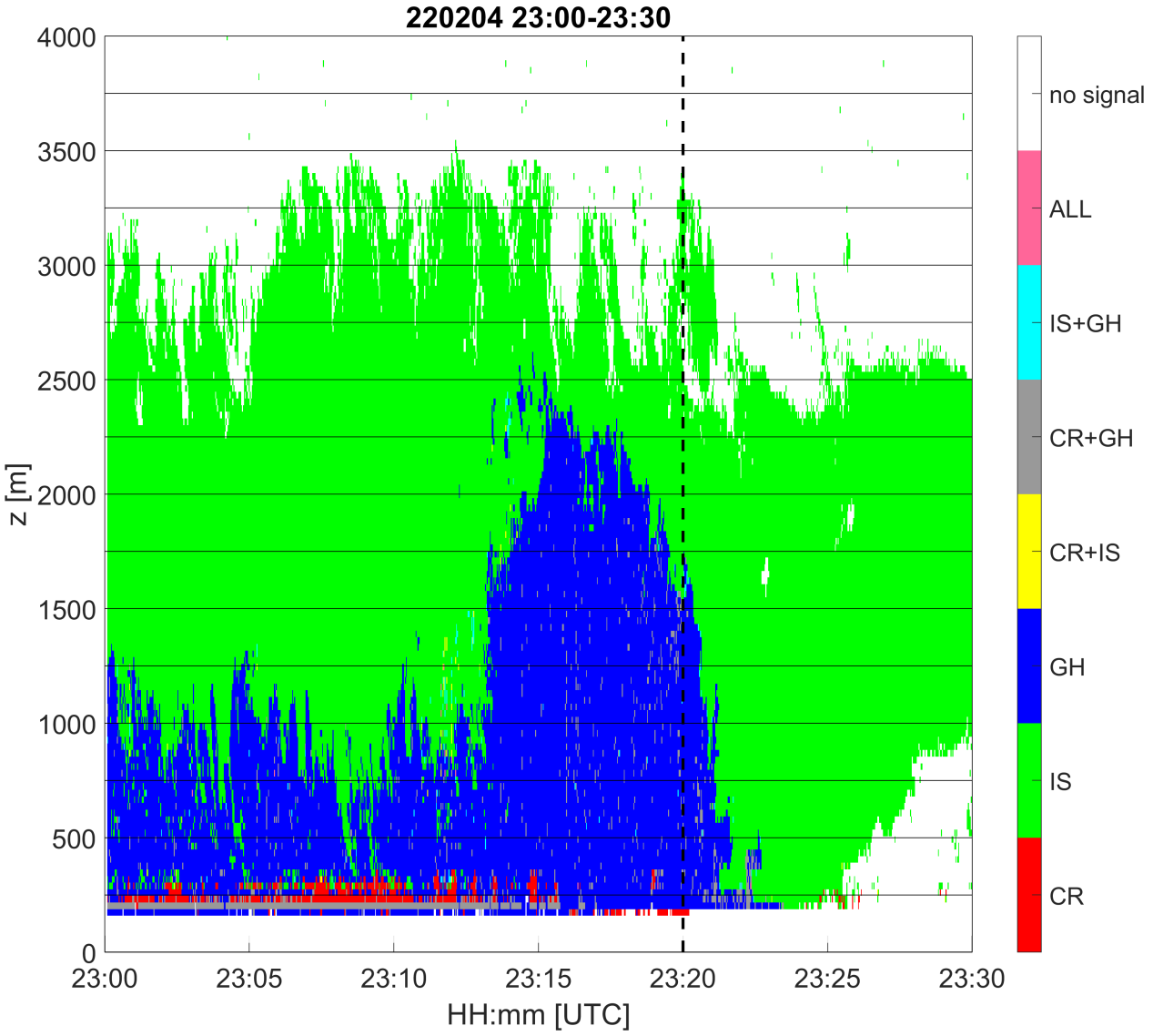

Figure 9. Hydrometeor classification using cloud profiler data based on Sokol et al. (2018). CR - Cloud and Raindrops, IS - Ice and Snow, GH - Graupel and Hail. Note sparse small gray areas (CR+GH) within the blue area (GH). For more details see Popová et al. (2023).

functions. Panel (b) represents the expected peak without discharge as it results from the best fit functions. Panel (c) shows SEVAN data during the low-intensity gamma-ray glow and its best fit function in 10 s summed bins (light markers represent data used for the function fitting, while dark markers display data not used for function fitting). Note that two markers of the strong gamma-ray glow are out of the y-axis range of the graph.

As visible in Figure **??**, the count rates follow the Gaussian curve up to the maximum of the gamma-ray glow, being still at the beginning of the Gaussian curve. However, we believe that our fitting is relevant because the fitted curve is similar to those previously observed in e.g., (Šlegl et al., 2022; Wada et al., 2019). If the gamma-ray glow had not been interrupted by the discharge and had continued following the Gaussian curve, the duration of the peak would be roughly 2.5 minutes, which aligns with the previous observations and the peak count rates of 5552 counts/s for SEVAN and 1448 counts/s for RT-56 with subtracted background, considering a wind speed of 10 m/s and a cloud base height less than 30 meters. The RT-56 fit differs from the SEVAN fit in the time of the maximum, but only by 1 second.

The continuation of the gamma-ray glow, if not terminated by the discharge, would correlate to the echo of aligned ice crystals by the electric field, as shown by the data from the Cloud profiler (Figure 8 - RHO). The continuation of such alignment of ice crystals in the upper part of the cloud can be explained by residually charged areas in the upper part of the cloud, above which the ice crystals were still caught in the electric field. Either the stroke did not discharge the upper charged region totally or not at all. This suggests the possibility of a horizontal discharge that left the upper charged region intact.

A question arises about the last 7 seconds (23:20:01.0-23:20:08.0) that preceded the discharge. As it does not follow the Gaussian curve, some mechanism must have prevented the gamma-ray glow from its full development. Such a sharp peak with a decrease before the end of the discharge was also observed by Wada et al. (2019).

3.2.1 Gamma-Ray Glow Spectrum

Gamma-ray spectrum measured by the RT-56 spectrometer: data during gamma-ray glow - blue (23:19:38 - 23:20:08 UTC), background - green (23:19:00 - 23:19:30 UTC), gamma-ray glow with subtracted background - red. Vertical error bars represent 1 σ error.

The gamma-ray glow spectrum detected by the spectrometer RT-56 follows the expected curve. Since the statistics at the very high energies (10-20 MeV) are poor, we can state that we detected an excess of photons with energies up to 10 MeV (Figure **??**).

4 Conclusions

The observation of a winter continental gamma-ray glow on Milešovka hill, Czechia, provides novel insights into thunderstorm-related radiation phenomena in a rarely studied environment. The findings reveal several important points:

1. **First Described Winter Gamma-Ray Glow in Continental Europe:** This event marks the first documented observation of a winter gamma-ray glow in Central Europe, a region where such phenomena are uncommon due to the rarity of winter thunderstorms with suitable conditions.

2. ~~**Unexpected Weak Electric Field During the Glow:** Despite the clear detection of high-energy gamma radiation, the corresponding electric field measured at the surface remained weak, challenging existing models that associate gamma-ray glows directly with significant electric field enhancements.~~

3. **Role of Ice Crystal Alignment in Radiation Generation:** Radar observations showed clear alignment of ice crystals in the cloud, indicative of a strong electric field higher up~~, even though this was not reflected in surface measurements~~. This suggests that strong localized electric fields within the cloud, rather than at the ground level, play a crucial role in generating gamma-ray glows.

4. **Unique Meteorological Conditions Contributing to the Event:** The exceptionally low cloud base and the relatively shallow vertical extent of the cloud allowed gamma radiation to reach the ground. This highlights how specific meteorological settings—like a low cloud base and limited cloud height—can influence the occurrence and detection of gamma-ray glows.

~~These results challenge conventional understanding and suggest the need for revised models that account for decoupling between ground-level electric fields and high-energy radiation processes within clouds.~~ The findings also underscore the value of combining multiple observational tools, such as cloud radar and an ionizing radiation ~~spectrometer~~detector, to unravel the complexities of thunderstorm dynamics and radiation generation in different climatic conditions.

Data availability. The cloud profiler data are described in Popová et al. (2023), The disdrometer, meteorological, and SEVAN data are available at **?**. link for reviewers https://data.mendeley.com/preview/c3tn4877gj?a=512b87b6-468b-4b99-8b83-754b96986d6f Graphs of latter mentioned data where produced by plotly Inc. (2015)

Author contributions. **J. Šlegl:** conceptualization, investigation, software, data curation, resources, visualisation, writing - original draft **Z. Sokol:** funding acquisition, software, methodology, visualization, writing - review & editing **P. Pešice:** investigation **R. Langer:** investigation **I. Strhárský:** software, resources **J. Popová:** resources, writing - review & editing **M. Kákona:** funding acquisition, resources, validation, writing - review & editing **I. Ambrožová:** supervision, writing - review & editing **O. Ploc:** supervision, funding acquisition, writing - review & editing

Competing interests. The authors declare that they have no known competing financial interests or personal relationships that could have appeared to influence the work reported in this paper.

Acknowledgements. This research was supported by the Johannes Amos Comenius Programme (OP JAC), project No. CZ.02.01.01/00/22_008/0004605 "Natural and anthropogenic georisks". We would like to thank the staff of the Milešovka observatory for the ongoing care of the equipment.

We would also like to express our sincere gratitude to Dr. Yuuki Wada for his comments and discussions, which greatly improved the quality and clarity of this research as well as to the other reviewer. We acknowledge BLIDS (Blitz Informationsdienst von Siemens) for providing us with the lightning data for the case study.

References

Brothers, M. D., Bruning, E. C., and Mansell, E. R.: Investigating the Relative Contributions of Charge Deposition and Turbulence in Organizing Charge within a Thunderstorm, Journal of the Atmospheric Sciences, 75, 3265 – 3284, https://doi.org/10.1175/JAS-D-18-0007.1, 2018.

Chilingarian, A. and Mkrtchyan, H.: Role of the Lower Positive Charge Region (LPCR) in initiation of the Thunderstorm Ground Enhancements (TGEs), Physical Review D - Particles, Fields, Gravitation and Cosmology, 86, 1–11, https://doi.org/10.1103/PhysRevD.86.072003, 2012.

Chilingarian, A., Hovsepyan, G., Arakelyan, K., Chilingaryan, S., Danielyan, V., Avakyan, K., Yeghikyan, A., Reymers, A., and Tserunyan, S.: Space environmental viewing and analysis network (SEVAN), Earth, Moon and Planets, 104, 195–210, https://doi.org/10.1007/s11038-008-9288-1, 2009.

Chilingarian, A., Daryan, A., Arakelyan, K., Hovhannisyan, A., Mailyan, B., Melkumyan, L., Hovsepyan, G., Chilingaryan, S., Reymers, A., and Vanyan, L.: Ground-based observations of thunderstorm-correlated fluxes of high-energy electrons, gamma rays, and neutrons, Physical Review D - Particles, Fields, Gravitation and Cosmology, 82, 1–11, https://doi.org/10.1103/PhysRevD.82.043009, 2010.

Chilingarian, A., Hovsepyan, G., and Hovhannisyan, A.: Particle bursts from thunderclouds: Natural particle accelerators above our heads, Physical Review D - Particles, Fields, Gravitation and Cosmology, 83, 1–11, https://doi.org/10.1103/PhysRevD.83.062001, 2011.

Chilingarian, A., Hovsepyan, G., Khanikyanc, G., Reymers, A., and Soghomonyan, S.: Lightning origination and thunderstorm ground enhancements terminated by the lightning flash, EPL, 110, https://doi.org/10.1209/0295-5075/110/49001, 2015.

Chilingarian, A., Hovsepyan, G., and Mnatsakanyan, E.: Mount Aragats as a stable electron accelerator for atmospheric high-energy physics research, Physical Review D, 93, 1–12, https://doi.org/10.1103/PhysRevD.93.052006, 2016.

Chilingarian, A., Hovsepyan, G., and Mailyan, B.: In situ measurements of the Runaway Breakdown (RB) on Aragats mountain, Nuclear Instruments and Methods in Physics Research, Section A: Accelerators, Spectrometers, Detectors and Associated Equipment, 874, 19–27, https://doi.org/10.1016/j.nima.2017.08.022, 2017.

Chilingarian, A., Hovsepyan, G., Karapetyan, G., and Zazyan, M.: Stopping muon effect and estimation of intracloud electric field, Astroparticle Physics, 124, 102 505, https://doi.org/10.1016/j.astropartphys.2020.102505, 2021a.

Chilingarian, A., Hovsepyan, G., Svechnikova, E., and Zazyan, M.: Electrical structure of the thundercloud and operation of the electron accelerator inside it, Astroparticle Physics, 132, 102 615, https://doi.org/10.1016/j.astropartphys.2021.102615, 2021b.

Chilingarian, A., Karapetyan, T., Zazyan, M., Hovsepyan, G., Sargsyan, B., Nikolova, N., Angelov, H., Chum, J., and Langer, R.: Maximum strength of the atmospheric electric field, Physical Review D, 103, 43 021, https://doi.org/10.1103/PhysRevD.103.043021, 2021c.

Chum, J., Langer, R., Baše, J., Kollárik, M., Strhárský, I., Diendorfer, G., and Rusz, J.: Significant enhancements of secondary cosmic rays and electric field at the high mountain peak of Lomnický Štít in High Tatras during thunderstorms, Earth, Planets and Space, 72, 28, https://doi.org/10.1186/s40623-020-01155-9, 2020.

Diniz, G., Wada, Y., Ohira, Y., Nakazawa, K., and Enoto, T.: Atmospheric Electron Spatial Range Extended by Thundercloud Electric Field Below the Relativistic Runaway Electron Avalanche Threshold, Journal of Geophysical Research: Atmospheres, 127, 1–14, https://doi.org/10.1029/2021JD035958, 2022.

Gurevich, A. V., Milikh, G. M., and Roussel-Dupre, R.: Runaway electron mechanism of air breakdown and preconditioning during a thunderstorm, Physics Letters A, 165, 463–468, https://doi.org/10.1016/0375-9601(92)90348-P, 1992.

Inc., P. T.: Collaborative data science, https://plot.ly, 2015.

Kelley, N. A., Smith, D. M., Dwyer, J. R., Splitt, M., Lazarus, S., Martinez-McKinney, F., Hazelton, B., Grefenstette, B., Lowell, A., and Rassoul, H. K.: Relativistic electron avalanches as a thunderstorm discharge competing with lightning, Nature Communications, 6, 7845, https://doi.org/10.1038/ncomms8845, 2015.

Kochkin, P., van Deursen, A. P., Marisaldi, M., Ursi, A., de Boer, A. I., Bardet, M., Allasia, C., Boissin, J. F., Flourens, F., Østgaard, N., van Deursen, A. P. J., Marisaldi, M., Ursi, A., de Boer, A. I., Bardet, M., Allasia, C., Boissin, J. F., Flourens, F., and Østgaard, N.: In-Flight Observation of Gamma Ray Glows by ILDAS, Journal of Geophysical Research: Atmospheres, 122, https://doi.org/10.1002/2017JD027405, 2017.

Kolmašová, I.: Comment on egusphere-2024-3075, https://doi.org/10.5194/egusphere-2024-3075-CC1, 2024.

Kolmašová, I., Santolík, O. O., Šlegl, J., Popová, J., Sokol, Z. Z., Zacharov, P., Ploc, O. O., Diendorfer, G., Langer, R., Lán, R., and Strhárský, I.: Continental thunderstorm ground enhancement observed at an exceptionally low altitude, Atmospheric Chemistry and Physics, 22, 7959–7973, https://doi.org/10.5194/acp-22-7959-2022, 2022.

Kudela, K., Chum, J., Kollárik, M., Langer, R., Strhárský, I., and Baše, J.: Correlations Between Secondary Cosmic Ray Rates and Strong Electric Fields at Lomnický štít, Journal of Geophysical Research: Atmospheres, 122, 10,700–10,710, https://doi.org/10.1002/2016JD026439, 2017.

McCarthy, M. and Parks, G. K.: Further observations of X-rays inside thunderstorms, Geophysical Research Letters, 12, 393–396, https://doi.org/10.1029/GL012i006p00393, 1985.

Melnikov, V., Zrnić, D. S., Weber, M. E., Fierro, A. O., and MacGorman, D. R.: Electrified Cloud Areas Observed in the SHV and LDR Radar Modes, Journal of Atmospheric and Oceanic Technology, 36, 151–159, https://doi.org/10.1175/JTECH-D-18-0022.1, 2019.

Munzar, J. and Franc, M.: Winter thunderstorms in central Europe in the past and the present, Atmospheric Research, 67-68, 501–515, https://doi.org/10.1016/S0169-8095(03)00062-0, 2003.

Popová, J., Sokol, Z., Wang, P., and Svoboda, J.: Observations and modelling of the winter thunderstorm on 4 February 2022 at the Milešovka meteorological observatory, Quarterly Journal of the Royal Meteorological Society, https://doi.org/10.1002/qj.4572, 2023.

Sokol, Z., Minářová, J., and Novák, P.: Classification of hydrometeors using measurements of the ka-band cloud radar installed at the Milešovka Mountain (Central Europe), Remote Sensing, 10, 1674, https://doi.org/10.3390/rs10111674, 2018.

Sokol, Z., Minářová, J., and Fišer, O.: Hydrometeor Distribution and Linear Depolarization Ratio in Thunderstorms, Remote Sensing, 12, 2144, https://doi.org/10.3390/rs12132144, 2020.

Torii, T., Sugita, T., Tanabe, S., Kimura, Y., Kamogawa, M., Yajima, K., and Yasuda, H.: Gradual increase of energetic radiation associated with thunderstorm activity at the top of Mt. Fuji, Geophysical Research Letters, 36, L13 804, https://doi.org/10.1029/2008GL037105, 2009.

Torii, T., Sugita, T., Kamogawa, M., Watanabe, Y., and Kusunoki, K.: Migrating source of energetic radiation generated by thunderstorm activity, Geophysical Research Letters, 38, 2–6, https://doi.org/10.1029/2011GL049731, 2011.

Tsuchiya, H., Enoto, T., Yamada, S., Yuasa, T., Kawaharada, M., Kitaguchi, T., Kokubun, M., Kato, H., Okano, M., Nakamura, S., and Makishima, K.: Detection of high-energy gamma rays from winter thunderclouds, Physical Review Letters, 99, 165 002, https://doi.org/10.1103/PhysRevLett.99.165002, 2007.

Tsuchiya, H., Enoto, T., Torii, T., Nakazawa, K., Yuasa, T., Torii, S., Fukuyama, T., Yamaguchi, T., Kato, H., Okano, M., Takita, M., and Makishima, K.: Observation of an energetic radiation burst from mountain-top thunderclouds, Physical Review Letters, 102, 10–13, https://doi.org/10.1103/PhysRevLett.102.255003, 2009.

Tsuchiya, H., Enoto, T., Yamada, S., Yuasa, T., Nakazawa, K., Kitaguchi, T., Kawaharada, M., Kokubun, M., Kato, H., Okano, M., and Makishima, K.: Long-duration γ ray emissions from 2007 and 2008 winter thunderstorms, Journal of Geophysical Research, 116, D09 113, https://doi.org/10.1029/2010JD015161, 2011.

Tsuchiya, H., Hibino, K., Kawata, K., Hotta, N., Tateyama, N., Ohnishi, M., Takita, M., Chen, D., Huang, J., Miyasaka, M., Kondo, I., Takahashi, E., Shimoda, S., Yamada, Y., Lu, H., Zhang, J. L., Yu, X. X., Tan, Y. H., Nie, S. M., Munakata, K., Enoto, T., and Makishima, K.: Observation of thundercloud-related gamma rays and neutrons in Tibet, Physical Review D - Particles, Fields, Gravitation and Cosmology, 85, https://doi.org/10.1103/PhysRevD.85.092006, 2012.

Tsuchiya, H., Enoto, T., Iwata, K., Yamada, S., Yuasa, T., Kitaguchi, T., Kawaharada, M., Nakazawa, K., Kokubun, M., Kato, H., Okano, M., Tamagawa, T., and Makishima, K.: Hardening and termination of long-duration γ rays detected prior to lightning, Physical Review Letters, 111, 1–5, https://doi.org/10.1103/PhysRevLett.111.015001, 2013.

Wada, Y., Bowers, G. S., Enoto, T., Kamogawa, M., Nakamura, Y., Morimoto, T., Smith, D. M., Furuta, Y., Nakazawa, K., Yuasa, T., Matsuki, A., Kubo, M., Tamagawa, T., Makishima, K., and Tsuchiya, H.: Termination of Electron Acceleration in Thundercloud by Intracloud/Intercloud Discharge, Geophysical Research Letters, 45, 5700–5707, https://doi.org/10.1029/2018GL077784, 2018.

Wada, Y., Enoto, T., Nakamura, Y., Furuta, Y., Yuasa, T., Nakazawa, K., Morimoto, T., Sato, M., Matsumoto, T., Yonetoku, D., Sawano, T., Sakai, H., Kamogawa, M., Ushio, T., Makishima, K., and Tsuchiya, H.: Gamma-ray glow preceding downward terrestrial gamma-ray flash, Communications Physics, 2, 3–6, https://doi.org/10.1038/s42005-019-0168-y, 2019.

Wada, Y., Enoto, T., Kubo, M., Nakazawa, K., Shinoda, T., Yonetoku, D., Sawano, T., Yuasa, T., Ushio, T., Sato, Y., Diniz, G. S., and Tsuchiya, H.: Meteorological Aspects of Gamma-Ray Glows in Winter Thunderstorms, Geophysical Research Letters, 48, 1–11, https://doi.org/10.1029/2020GL091910, 2021a.

Wada, Y., Matsumoto, T., Enoto, T., Nakazawa, K., Yuasa, T., Furuta, Y., Yonetoku, D., Sawano, T., Okada, G., Nanto, H., Hisadomi, S., Tsuji, Y., Diniz, G. S., Makishima, K., and Tsuchiya, H.: Catalog of gamma-ray glows during four winter seasons in Japan, Physical Review Research, 3, https://doi.org/10.1103/PhysRevResearch.3.043117, 2021b.

Wada, Y., Tsurumi, M., Hayashi, S., and Michimoto, K.: Synoptic meteorological conditions of gamma-ray glows in winter thunderstorms, Progress in Earth and Planetary Science, 10, https://doi.org/10.1186/s40645-023-00538-2, 2023.

Wanke, E.: Blitzortung.org A low cost Time of Arrival Lightning Location Network, https://www.blitzortung.org/Compendium/Documentations/Documentation_2010-11-03_Green_PCB_6.5_PCB_5.5.pdf, 2010.

Williams, E., Mkrtchyan, H., Mailyan, B., Karapetyan, G., and Hovakimyan, S.: Radar Diagnosis of the Thundercloud Electron Accelerator, Journal of Geophysical Research: Atmospheres, 127, https://doi.org/10.1029/2021JD035957, 2022.

Šlegl, J., Langer, R., Brunclík, T., Mašek, P., Strhárský, I., Ambrožová, I., Chum, J., and Ploc, O.: Spectrometry of High-Energy Photons on High Mountain Observatory Lomnický Štít During Thunderstorms, Radiation protection dosimetry, 198, 623–627, https://doi.org/10.1093/rpd/ncac108, 2022.